Report Title: Electromagnetic Scattering and Radiation from
                                         Microstrip Patch Antennas and Arrays Residing
                                         in a Cavity

Report Authors: Jian-Ming Jin and John L. Volakis

Primary University Collaborator: John L. Volakis

Primary NASA-Ames Collaborator: Alex Woo

University Address: Radiation Laboratory
                                          Department of Electrical Engineering
                                          and Computer Science
                                          The University of Michigan
                                          Ann Arbor, MI 48109-2122

Date: August 15, 1990

en m

UMROMMO

ABSTRACT

A hybrid numerical technique is proposed for a characterization of the scattering and radiation properties of microstrip patch antennas and arrays residing in a cavity which is, in turn, recessed in a ground plane. The technique combines the finite element and boundary integral methods to formulate a system for the solution of the fields at the aperture and those inside the cavity. By virtue of the finite element method, the proposed technique is applicable to patch antennas and arrays residing on or embedded in the dielectric substrate. Also, the technique is capable of treating various feed structures. In this report, we develop the formulation and describe the pertinent numerical implementation. Numerical examples are also presented demonstrating the validity, versatility and capability of the technique.

OBJECTIVE

The ultimate objective of this project is to develop a new technique which permits an accurate simulation of microstrip patch antennas or arrays with various feed, superstrate and/or substrate configurations residing in a cavity recessed in a ground plane (An example of such a structure is given in Figure 1). The technique combines the finite element and boundary integral methods to formulate a system suitable for solution via the conjugate gradient method in conjunction with the fast Fourier transform. The final code is intended to compute both scattering and radiation patterns of the structure with an affordable memory demand.
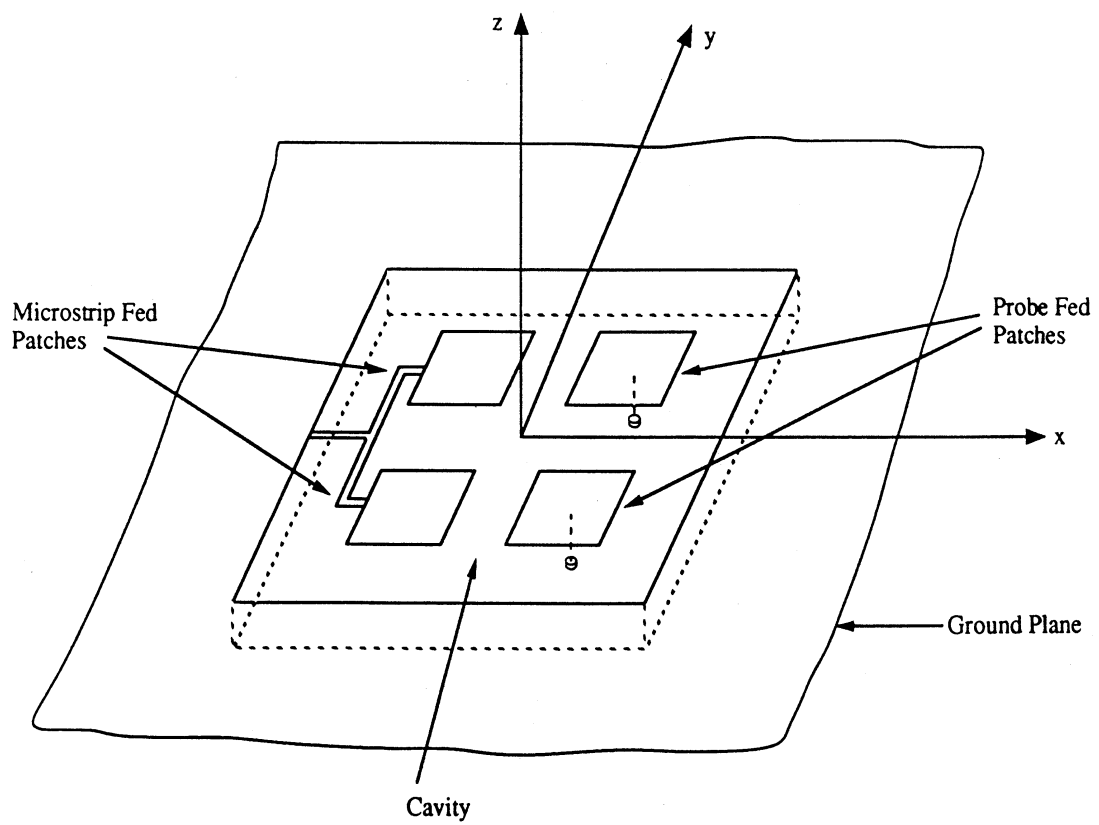
1

Figure 1: Geometry of a microstrip patch array in a cavity.

BACKGROUND

Electromagnetic scattering and radiation from microstrip patch antennas and arrays is an important problem having many practical applications. However, although well documented methodologies exist for analysis of patch antennas with infinite superstrate and/or substrates [1], there is no well established method to treat those residing in a cavity (see Figure 1) as is the case with airborne deployments.

Recently, a new technique which combines the finite element and boundary integral formulations to yield a system for solution via the conjugate gradient method (CGM) and the fast Fourier transform (FFT) was proposed for electromagnetic scattering computations. In particular, the method was formulated for the characterization of filled slots and grooves in a thick ground plane with transverse electric (TE) and transverse magnetic (TM) incidence [2], [3]. This technique was later extended for a characterization of three-dimensional cavity-backed apertures in a ground plane [4] and slots in a thick conducting plane [5]. In this report we describe an extension of this technique for the electromagnetic characterization of the scattering and radiation from the microstrip patch antennas and arrays residing in a cavity.

The presented technique invokes the equivalence principle [6] to subdivide the original problem into two equivalent problems which are then coupled by enforcing field continuity. The fields in each region are subsequently formulated via a variational or integral equation approach leading to a coupled set of integral equations solved via the finite element method [7]. By virtue of the finite element method, the technique is applicable to patch antennas residing on or embedded in the substrate. In the following sections the proposed hybrid formulation is discussed in some detail along with the pertinent

discretization of the resulting integral equations. Somef results are also presented for validation purposes.

PROGRESS

A. Formulation

Consider the three-dimensional structure illustrated in Figure 1. The specific configuration consists of some microstrip patch antennas residing on or embedded in the substrate. The whole structure is residing in a cavity which is recessed in a ground plane. We will denote the free space region above the plane ($z > 0$) as region I and that inside the cavity ($-t < z < 0$) as region II occupying the volume V. We will further assume that the cavity is filled with an inhomogeneous material having a relative permittivity $\epsilon_r(\mathbf{r})$ and relative permeability $\mu_r(\mathbf{r})$.

In accordance with the equivalence principle [6], the fields in the two regions can be decoupled by closing the aperture with a perfect conductor and introducing the equivalent magnetic current

$$\mathbf{M} = \mathbf{E} \times \hat{\mathbf{z}} \tag{1}$$

over the extent of the aperture, where $\mathbf{E}$ is the electric field at the aperture ($z = 0$). The field in region I is then due to the radiation caused by the equivalent current $\mathbf{M}$ residing on the ground plane and possibly by other impressed external sources ($\mathbf{J}_e$, $\mathbf{M}_e$) in the upper half space. Accordingly, by invoking image theory we have

$$\mathbf{H}^I(\mathbf{r}) = \mathbf{H}^i(\mathbf{r}) + \mathbf{H}^r(\mathbf{r}) - 2jk_0Y_0 \iint_S \bar{\bar{\mathbf{G}}}_0(\mathbf{r},\mathbf{r}') \cdot \mathbf{M}(\mathbf{r}')dS' \tag{2}$$

4

where $\mathbf{H}^i$ denotes the incident field due to $(\mathbf{J}_e, \mathbf{M}_e)$ and $\mathbf{H}^r$ is that reflected by the ground plane without the aperture. Also, $k_0 = 2\pi/\lambda$ is the free space wavenumber, $Z_0 = 1/Y_0$ is the free space intrinsic impedance, S denotes the planar surface area of the aperture and $\bar{\bar{G}}_0$ is the free-space dyadic Green's function given by

$$\bar{\bar{G}}_0(\mathbf{r},\mathbf{r}') = \left(\bar{\bar{I}} + \frac{1}{k_0^2}\nabla\nabla \right) G_0(\mathbf{r},\mathbf{r}') \tag{3}$$

with

$$\bar{\bar{I}} = \hat{x}\hat{x} + \hat{y}\hat{y} + \hat{z}\hat{z} \quad \text{and} \quad G_0(\mathbf{r},\mathbf{r}') = \frac{e^{-jk_0|\mathbf{r}-\mathbf{r}'|}}{4\pi|\mathbf{r}-\mathbf{r}'|}.$$

Note, however, that when the antenna is in the radiation mode, no external sources $(\mathbf{J}_e, \mathbf{M}_e)$ exist and, therefore, the first two terms on the right hand side of (2) disappear.

Enforcing continuity of the tangential electric fields across the aperture, we find that the field in region II can be represented by the radiation of the equivalent magnetic current $-\mathbf{M}$ and other impressed internal sources $(\mathbf{J}_i, \mathbf{M}_i)$ which can be used to model various feed structures. The fields in the two regions are then coupled by enforcing continuity of the tangential magnetic fields across the aperture. This gives

$$\hat{z} \times \mathbf{H}^I(\mathbf{M}, \mathbf{J}_e, \mathbf{M}_e) = \hat{z} \times \mathbf{H}^{II}(-\mathbf{M}, \mathbf{J}_i, \mathbf{M}_i) \quad \text{at } z = 0 \tag{4}$$

where $\mathbf{H}^I$ and $\mathbf{H}^{II}$ denote the magnetic fields in regions I and II, respectively.

The fields in the cavity region (region II) can be formulated using the finite element method. Specifically, the cavity fields are demanded to satisfy the variational equation

$$\delta F = 0 \tag{5}$$

5

where the functional F is given by

$$F\left(\mathbf{E}^{II}\right) = \frac{1}{2} \iiint_V \left[\frac{1}{\mu_r}\left(\nabla \times \mathbf{E}^{II}\right) \bullet \left(\nabla \times \mathbf{E}^{II}\right) - k_0^2 \epsilon_r \mathbf{E}^{II} \bullet \mathbf{E}^{II}\right] dV$$
$$+ \iiint_V \left[jk_0 Z_0 \mathbf{J}_i \bullet \mathbf{E}^{II} - \frac{1}{\mu_r}\mathbf{M}_i \bullet \left(\nabla \times \mathbf{E}^{II}\right)\right] dV$$
$$+ jk_0 Z_0 \oiint_{S_{cav}} \left(\mathbf{E}^{II} \times \mathbf{H}^{II}\right) \bullet \hat{n} dS \tag{6}$$

if the variation is taken with respect to the electric field. In (6), V denotes the volume occupied by region II, S_{cav} corresponds to the surface that encloses V and $\hat{n}$ denotes the unit vector normal to the surface, pointing away from the cavity. The second volume integral represents the radiation of the impressed internal sources ($\mathbf{J}_i$, $\mathbf{M}_i$).

To solve (6), it is necessary that the fields be known over the surface specified by S_{cav}. Obviously, the boundary condition to be imposed on the conducting boundaries of the cavity and also on the surface of the patch antennas is

$$\hat{n} \times \mathbf{E}^{II} = 0 \tag{7}$$

Substituting this into (6) eliminates the portion of the surface integral over the conducting boundary of the cavity (that is, there is no power flow through the metallic portion of S_{cav}). It remains to specify the boundary condition over the cavity's aperture and this is given by (1). Enforcing the continuity condition (4), we obtain

$$F = \frac{1}{2} \iiint_V \left[\frac{1}{\mu_r}\left(\nabla \times \mathbf{E}^{II}\right) \bullet \left(\nabla \times \mathbf{E}^{II}\right) - k_0^2 \epsilon_r \mathbf{E}^{II} \bullet \mathbf{E}^{II}\right] dV$$
$$+ \iiint_V \left[jk_0 Z_0 \mathbf{J}_i \bullet \mathbf{E}^{II} - \frac{1}{\mu_r}\mathbf{M}_i \bullet \left(\nabla \times \mathbf{E}^{II}\right)\right] dV$$
$$- 2k_0^2 \iint_S \mathbf{M}(\mathbf{r}) \bullet \left[\iint_S \bar{\bar{\mathbf{G}}}_0(\mathbf{r},\mathbf{r}') \bullet \mathbf{M}(\mathbf{r}')dS'\right] dS$$
$$- jk_0 Z_0 \iint_S \mathbf{M}(\mathbf{r}) \bullet \left[\mathbf{H}^i(\mathbf{r}) + \mathbf{H}^r(\mathbf{r})\right] dS \tag{8}$$

which can be discretized via the finite element method for a solution of M and the internal field $\mathbf{E}^{II}$. Once M is found, the far zone scattered or radiated field can be easily computed from

$$\mathbf{H}^s(\mathbf{r}) = -jk_0Y_0\frac{e^{-jk_0r}}{2\pi r}\iint_S(\hat{\theta}\hat{\theta} + \hat{\phi}\hat{\phi}) \bullet \mathbf{M}(x',y')e^{jk_0\sin\theta(x'\cos\phi+y'\sin\phi)}dx'dy' \qquad (9)$$

where (r,θ,ϕ) are the usual spherical coordinates of the observation point. The radar cross section (RCS) of the structure is then given by

$$\sigma = \lim_{r\to\infty} 4\pi r^2\frac{|\mathbf{H}^s(\mathbf{r})|^2}{|\mathbf{H}^i(\mathbf{r})|^2}. \qquad (10)$$

The input impedance and antenna gain can also obtained from the solution of $\mathbf{E}^{II}$.

B. Discretization

For a numerical implementation of (5) we must first discretize the functionals by subdividing V and S into smaller volume and surface elements, respectively. Considering (8), it is convenient to rewrite the functional F as

$$F = F_V + F_S + F_I + F_E \qquad (11)$$

where F_V is the volume integral

$$F_V = \frac{1}{2}\iiint_V \left\{\frac{1}{\mu_r}\left[\left(\frac{\partial E_z}{\partial y} - \frac{\partial E_y}{\partial z}\right)^2 + \left(\frac{\partial E_x}{\partial z} - \frac{\partial E_z}{\partial x}\right)^2 + \left(\frac{\partial E_y}{\partial x} - \frac{\partial E_x}{\partial y}\right)^2\right] \right.$$
$$\left. -k_0^2\epsilon_r\left(E_x^2 + E_y^2 + E_z^2\right)\right\}dV \qquad (12)$$

obtained by expanding the appropriate integrand in (8) and F_S denotes the surface integral

$$F_S = -2k_0^2\iint_S \mathbf{M}(\mathbf{r}) \bullet \left[\iint_S \bar{\bar{\mathbf{G}}}_0(\mathbf{r},\mathbf{r}') \bullet \mathbf{M}(\mathbf{r}')dS'\right] dS. \qquad (13)$$

The remaining portion of F is associated with the sources and is given by

$$F_I = \iiint_V \left[jk_0 Z_0 \mathbf{J}_i \bullet \mathbf{E} - \frac{1}{\mu_r} \mathbf{M}_i \bullet (\nabla \times \mathbf{E}) \right] dV \tag{14}$$

and

$$F_E = -2jk_0 Z_0 \iint_S \mathbf{M}(\mathbf{r}) \bullet \mathbf{H}^i(\mathbf{r}) dS \tag{15}$$

upon using the relation $\hat{z} \times \mathbf{H}^r(\mathbf{r}) = \hat{z} \times \mathbf{H}^i(\mathbf{r})$. For simplicity, we have omitted the superscript II and this practice will be continued in the remaining portion of the report.

To discretize (12) we subdivide the volume V into M_v small volume elements such as tetrahedra, triangular prisms, or rectangular bricks. The ideal element for the discretization of rectangular cavities or those that can be modelled as a collection of rectangular volumes is the rectangular brick illustrated in Figure 2. An example of the finite element mesh using rectangular bricks is given in Figure 3. For arbitrarily shaped cavities, triangular prisms and tetrahedra may be used but in this report we restrict our attention to rectangular bricks. Consider the rectangular brick of dimensions $a \times b \times c$, representing the eth element, as illustrated in Figure 2. The field components within this element may be expressed as

$$E_x = \sum_{j=1}^{4} N_{xj}^e(y,z)\phi_{xj}^e \;\; ; \;\; E_y = \sum_{j=1}^{4} N_{yj}^e(z,x)\phi_{yj}^e \;\; ; \;\; E_z = \sum_{j=1}^{4} N_{zj}^e(x,y)\phi_{zj}^e \tag{16}$$

where N_{xj}^e, N_{yj}^e and N_{zj}^e are the expansion or shape functions given by

$$N_{x1}^e = \frac{(b-y')(c-z')}{bc} \;\; ; \;\; N_{x2}^e = \frac{y'(c-z')}{bc} \;\; ; \;\; N_{x3}^e = \frac{(b-y')z'}{bc} \;\; ; \;\; N_{x4}^e = \frac{y'z'}{bc}$$

$$N_{y1}^e = \frac{(c-z')(a-x')}{ca} \;\; ; \;\; N_{y2}^e = \frac{z'(a-x')}{ca} \;\; ; \;\; N_{y3}^e = \frac{(c-z')x'}{ca} \;\; ; \;\; N_{y4}^e = \frac{z'x'}{ca}$$

$$N_{z1}^e = \frac{(a-x')(b-y')}{ab} \;\; ; \;\; N_{z2}^e = \frac{x'(b-y')}{ab} \;\; ; \;\; N_{z3}^e = \frac{(a-x')y'}{ab} \;\; ; \;\; N_{z4}^e = \frac{x'y'}{ab}$$
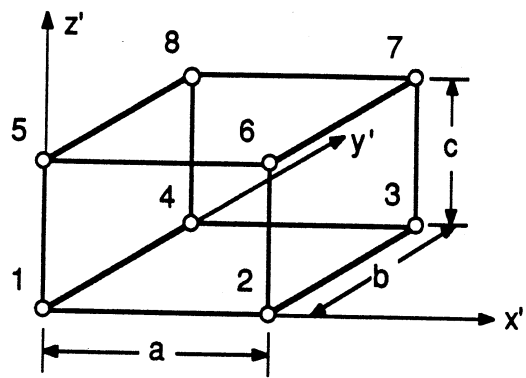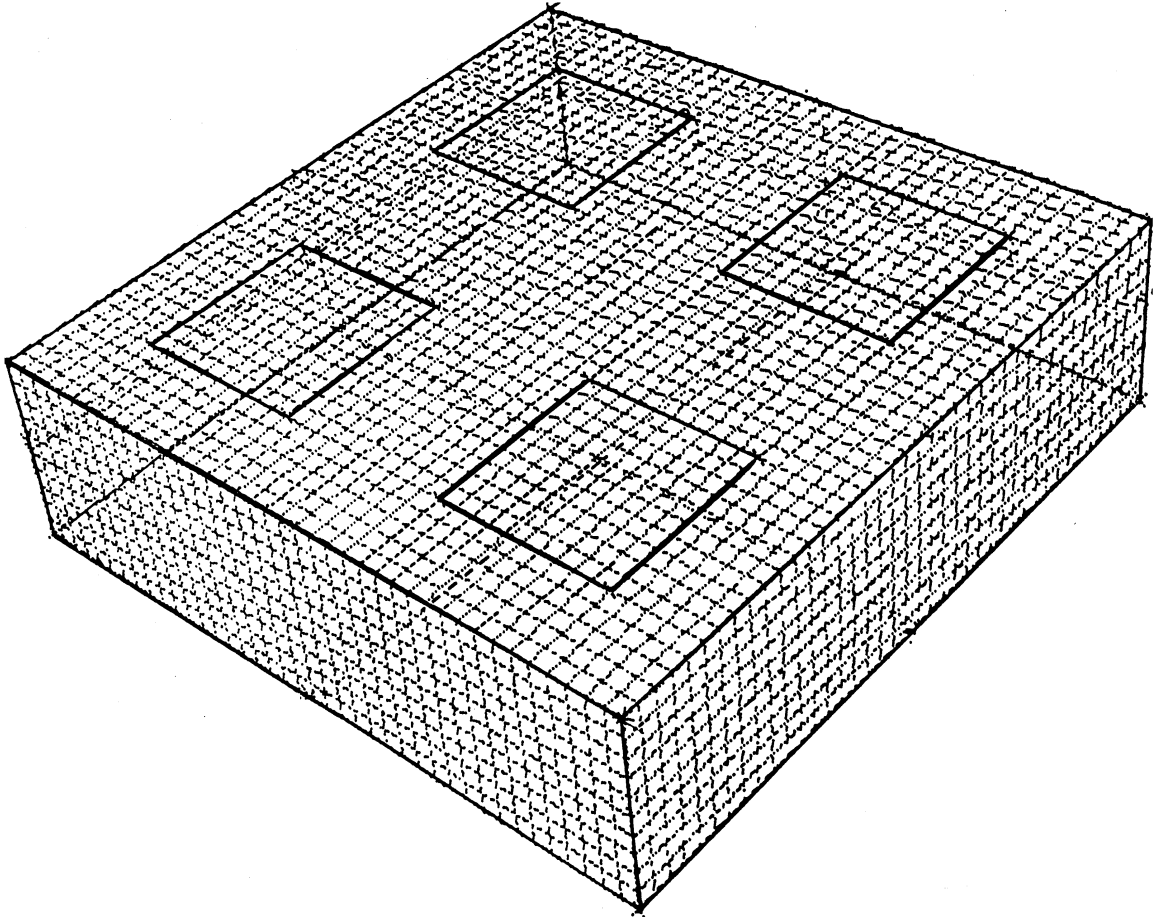
8

Figure 2: A rectangular brick.

Figure 3: Finite element mesh for a cavity with four patches.

In these, (x', y', z') denote the local coordinates specifying a point within the eth element and from an examination of the expansion functions we observe that ϕ_{x1}^e represents an average of the field component E_x along the edge segment (1,2). Likewise, ϕ_{x2}^e is associated with the E_x component along the edge (3,4), ϕ_{x3}^e corresponds to the E_x component along the edge (5,6) and ϕ_{x4}^e is associated with the E_x component along the edge (7,8). Similar identifications can, of course, be made for ϕ_{yj}^e and ϕ_{zj}^e. Therefore, N_{xj}^e, N_{yj}^e and N_{zj}^e can be termed as edge-based expansion functions, in contrast to the traditional node-based expansion functions employed in [4]. A feature of these functions is that they satisfy the divergence condition within the volume of the element and this permits the elimination of the penalty term discussed in [4]. Also, the edge-based functions allow a convenient enforcement of the required boundary conditions at the dielectric interfaces and conducting walls. Furthermore, the edge-based functions avoid an explicit specification of the fields at the corners and edges, where these may be singular [8]. This is not, however, permitted when employing the node-based expansion functions unless special basis functions (which model the singular behavior of the fields) are incorporated into the formulation leading to a much more complicated implementation.

Substituting (16) into (12) yields the portion of F_V attributed to the eth element. The complete expression for F_V is then obtained by summing/assembling the contributions from all elements. This yields a functional in terms of the unknown field components which must be found to satisfy (5). In accordance with the Rayleigh-Ritz procedure this is equivalent to setting the derivatives of F with respect to the fields ϕ_{pj}^e $(p = x, y, z)$ equal to zero. Differentiating the portion of F_V attributed to the eth element with

11

respect to the field ϕ_{xi}^e we obtain

$$\frac{\partial F_V^e}{\partial \phi_{xi}^e} = \sum_{j=1}^{4} \iiint_{V^e} \frac{1}{\mu_r} \left\{ \left[\frac{\partial N_{xi}^e}{\partial y} \frac{\partial N_{xj}^e}{\partial y} + \frac{\partial N_{xi}^e}{\partial z} \frac{\partial N_{xj}^e}{\partial z} - k_0^2 \epsilon_r \mu_r N_{xi}^e N_{xj}^e \right] \phi_{xj}^e \right.$$
$$\left. - \frac{\partial N_{xi}^e}{\partial y} \frac{\partial N_{yj}^e}{\partial x} \phi_{yj}^e - \frac{\partial N_{xi}^e}{\partial z} \frac{\partial N_{zj}^e}{\partial x} \phi_{zj}^e \right\} dV. \tag{17}$$

Similarly, by differentiating with respect to the other field components we have

$$\frac{\partial F_V^e}{\partial \phi_{yi}^e} = \sum_{j=1}^{4} \iiint_{V^e} \frac{1}{\mu_r} \left\{ -\frac{\partial N_{yi}^e}{\partial x} \frac{\partial N_{xj}^e}{\partial y} \phi_{xj}^e + \left[\frac{\partial N_{yi}^e}{\partial x} \frac{\partial N_{yj}^e}{\partial x} + \frac{\partial N_{yi}^e}{\partial z} \frac{\partial N_{yj}^e}{\partial z} \right. \right.$$
$$\left. \left. - k_0^2 \epsilon_r \mu_r N_{yi}^e N_{yj}^e \right] \phi_{yj}^e - \frac{\partial N_{yi}^e}{\partial z} \frac{\partial N_{zj}^e}{\partial y} \phi_{zj}^e \right\} dV \tag{18}$$

and

$$\frac{\partial F_V^e}{\partial \phi_{zi}^e} = \sum_{j=1}^{4} \iiint_{V^e} \frac{1}{\mu_r} \left\{ -\frac{\partial N_{zi}^e}{\partial x} \frac{\partial N_{xj}^e}{\partial z} \phi_{xj}^e - \frac{\partial N_{zi}^e}{\partial y} \frac{\partial N_{yj}^e}{\partial z} \phi_{yj}^e \right.$$
$$\left. + \left[\frac{\partial N_{zi}^e}{\partial x} \frac{\partial N_{zj}^e}{\partial x} + \frac{\partial N_{zi}^e}{\partial y} \frac{\partial N_{zj}^e}{\partial y} - k_0^2 \epsilon_r \mu_r N_{zi}^e N_{zj}^e \right] \phi_{zj}^e \right\} dV. \tag{19}$$

We observe that if ϵ_r and μ_r are assumed constant within the eth element, all integrals in (17)-(19) can be evaluated analytically. Otherwise, a numerical integration may be required for their evaluation.

Let us now consider the discretization of the surface integral in (13). A difficulty in the evaluation of this integral is the usual singularity associated with the derivatives of the free space Green's function. This, however, can be avoided by transfering the derivatives to the current. To do so, we invoke a common vector identity and the divergence theorem, leading to

$$F_S = -2 \iint_S \mathbf{M}(\mathbf{r}) \bullet \left[k_0^2 \iint_S \mathbf{M}(\mathbf{r}') G_0(\mathbf{r}, \mathbf{r}') dS' \right.$$
$$\left. + \nabla \iint_S \nabla' \bullet \mathbf{M}(\mathbf{r}') G_0(\mathbf{r}, \mathbf{r}') dS' \right] dS. \tag{20}$$

12

Through the same process, (20) can be further rewritten as

$$
F_S = -2k_0^2 \iint_S \mathbf{M}(\mathbf{r}) \bullet \left[\iint_S \mathbf{M}(\mathbf{r}')G_0(\mathbf{r},\mathbf{r}')dS' \right] dS
$$

$$
+2 \iint_S \nabla \bullet \mathbf{M}(\mathbf{r}) \left[\iint_S \nabla' \bullet \mathbf{M}(\mathbf{r}')G_0(\mathbf{r},\mathbf{r}')dS' \right] dS \tag{21}
$$

and by invoking (1) we obtain

$$
F_S = -2k_0^2 \iint_S E_x \left[\iint_S E_x G_0 dS' \right] dS - 2k_0^2 \iint_S E_y \left[\iint_S E_y G_0 dS' \right] dS
$$

$$
+2 \iint_S \left(\frac{\partial E_x}{\partial y} - \frac{\partial E_y}{\partial x} \right) \left[\iint_S \left(\frac{\partial E_x}{\partial y'} - \frac{\partial E_y}{\partial x'} \right) G_0 dS' \right] dS \tag{22}
$$

which can be discretized by subdividing S into M_s smaller surface elements. Substituting (16) into (22) and replacing S in the first pair of integrals with S^e, the area of the eth surface element, gives the portion of F_S attributed to the eth element. As noted earlier, to enforce the stationarity condition we need the derivatives of F_S with respect to the fields ϕ_{xi}^e and ϕ_{yi}^e. For the eth element we have

$$
\frac{\partial F_S^e}{\partial \phi_{xi}^e} = -2k_0^2 \iint_{S^e} N_{xi}^e \left[\sum_{e=1}^{M_s} \sum_{j=1}^{2} \phi_{xj}^e \iint_{S^e} N_{xj}^e G_0 dS' \right] dS
$$

$$
+2 \iint_{S^e} \frac{\partial N_{xi}^e}{\partial y} \left[\sum_{e=1}^{M_s} \sum_{j=1}^{2} \iint_{S^e} \left(\frac{\partial N_{xj}^e}{\partial y'} \phi_{xj}^e - \frac{\partial N_{yj}^e}{\partial x'} \phi_{yj}^e \right) G_0 dS' \right] dS, \tag{23}
$$

$$
\frac{\partial F_S^e}{\partial \phi_{yi}^e} = -2k_0^2 \iint_{S^e} N_{yi}^e \left[\sum_{e=1}^{M_s} \sum_{j=1}^{2} \phi_{yj}^e \iint_{S^e} N_{yj}^e G_0 dS' \right] dS
$$

$$
-2 \iint_{S^e} \frac{\partial N_{yi}^e}{\partial x} \left[\sum_{e=1}^{M_s} \sum_{j=1}^{2} \iint_{S^e} \left(\frac{\partial N_{xj}^e}{\partial y'} \phi_{xj}^e - \frac{\partial N_{yj}^e}{\partial x'} \phi_{yj}^e \right) G_0 dS' \right] dS \tag{24}
$$

and $\partial F_S^e / \partial \phi_{zi}^e = 0$ since F_S is not a function of E_z. We note that in deriving (23) and (24) the differentiation was performed only with respect to the node fields outside the square brackets in (22) while those introduced by substituting (2) into (6) remained uneffected.

It remains to discretize (14) and (15) which involve the excitation fields. Let us consider (14) first. By expanding the integrand in (14), we have

$$F_I = jk_0Z_0 \iiint_V (E_x J_{ix} + E_y J_{iy} + E_z J_{iz})\, dV - \iiint_V \frac{1}{\mu_r}\left[\left(\frac{\partial E_z}{\partial y} - \frac{\partial E_y}{\partial z}\right) M_{ix}\right.$$
$$\left. + \left(\frac{\partial E_x}{\partial z} - \frac{\partial E_z}{\partial x}\right) M_{iy} + \left(\frac{\partial E_y}{\partial x} - \frac{\partial E_x}{\partial y}\right) M_{iz}\right] dV \quad (25)$$

By introducing the expansion (16), we obtain

$$\frac{\partial F_I^e}{\partial \phi_{xi}^e} = jk_0Z_0 \iiint_{V^e} N_{xi}^e J_{ix}\, dV - \iiint_{V^e} \frac{1}{\mu_r}\left(\frac{\partial N_{xi}}{\partial z} M_{iy} - \frac{\partial N_{xi}}{\partial y} M_{iz}\right) dV, \quad (26)$$

$$\frac{\partial F_I^e}{\partial \phi_{yi}^e} = jk_0Z_0 \iiint_{V^e} N_{yi}^e J_{iy}\, dV - \iiint_{V^e} \frac{1}{\mu_r}\left(\frac{\partial N_{yi}}{\partial x} M_{iz} - \frac{\partial N_{yi}}{\partial z} M_{ix}\right) dV, \quad (27)$$

and

$$\frac{\partial F_I^e}{\partial \phi_{zi}^e} = jk_0Z_0 \iiint_{V^e} N_{zi}^e J_{iz}\, dV - \iiint_{V^e} \frac{1}{\mu_r}\left(\frac{\partial N_{zi}}{\partial y} M_{ix} - \frac{\partial N_{zi}}{\partial x} M_{iy}\right) dV. \quad (28)$$

Now let us consider (15). By replacing **M** with **E** in accordance with (1) we obtain

$$F_E = 2jk_0Z_0 \iint_S \left(E_x H_y^i - E_y H_x^i\right) dS. \quad (29)$$

This can again be discretized by introducing the expansion (16) and by doing so we obtain (for the eth element)

$$\frac{\partial F_E^e}{\partial \phi_{xi}^e} = 2jk_0Z_0 \iint_{S^e} N_{xi}^e H_y^i\, dS \quad (30)$$

and

$$\frac{\partial F_E^e}{\partial \phi_{yi}^e} = -2jk_0Z_0 \iint_{S^e} N_{yi}^e H_x^i\, dS \quad (31)$$

14

Given the partial derivatives of all integral functions comprising the functional F we can now proceed with the construction of the final system of equations by imposing the stationarity condition (5). This implies that

$$\frac{\partial F}{\partial \phi_{xi}} = \sum_{e=1}^{M_v} \frac{\partial F_V^e}{\partial \phi_{xi}^e} + \sum_{e=1}^{M_v} \frac{\partial F_I^e}{\partial \phi_{xi}^e} + \sum_{e=1}^{M_s} \frac{\partial F_S^e}{\partial \phi_{xi}^e} + \sum_{e=1}^{M_s} \frac{\partial F_E^e}{\partial \phi_{xi}^e} = 0 \tag{32}$$

$$i = 1, 2, 3, ..., N_x$$

$$\frac{\partial F}{\partial \phi_{yi}} = \sum_{e=1}^{M_v} \frac{\partial F_V^e}{\partial \phi_{yi}^e} + \sum_{e=1}^{M_v} \frac{\partial F_I^e}{\partial \phi_{yi}^e} + \sum_{e=1}^{M_s} \frac{\partial F_S^e}{\partial \phi_{yi}^e} + \sum_{e=1}^{M_s} \frac{\partial F_E^e}{\partial \phi_{yi}^e} = 0 \tag{33}$$

$$i = 1, 2, 3, ..., N_y$$

$$\frac{\partial F}{\partial \phi_{zi}} = \sum_{e=1}^{M_v} \frac{\partial F_V^e}{\partial \phi_{zi}^e} + \sum_{e=1}^{M_v} \frac{\partial F_I^e}{\partial \phi_{zi}^e} = 0 \tag{34}$$

$$i = 1, 2, 3, ..., N_z$$

leading to a matrix system for the solution of the node fields. In (32), N_x denotes the total number of element edges parallel to the x-axis and similar definitions hold for N_y and N_z. Also, ϕ_{pi} ($p = x, y, z$) are the fields labelled with global indices and as before ϕ_{pi}^e ($p = x, y, z$) are the fields associated with the eth volume or surface element. Both ϕ_{pi} and ϕ_{pi}^e refer to the field at the same edge and thus the eth term of the summations has non-zero value only if the global edge i belongs to the eth element. The system implied by (32)-(34) must, of course, be solved after imposing the boundary condition (7) which permits us to zero out those field components that belong to edges on metallic boundaries. This reduces substantially the number of unknowns in the system which can then be solved via direct inversion, LU decomposition, or iteration. However, since the system matrix is partly full and partly sparse as well as symmetric and banded (if the nodes are properly numbered), it can be more efficiently solved by those algorithms which exploit these properties [9]. Various partition techniques such as the those discussed in

[10] can also be employed to enhance the efficiency of the solution. Further, the matrix system is amenable to a conjugate gradient – fast Fourier transform solution, thus, reducing the memory demand to $O(N)$ as in [2], [3].

C. Results

Based on the formulation and implementation procedure described above, a computer code was developed for scattering computations. The code has been validated for cavity and slot scattering by comparing the results with those obtained using the moment method and the mode matching method. A variety of comparisons can be found in [4] and [5]. Here we present a comparison of our numerical solution with measured data. Figure 4 shows the backscatter pattern for a cavity which is 16 inch long, 0.1968 inch wide and 0.837 inch deep. The measurement was performed at 12 GHz [11] and it is seen that the numerical results agree with the measured data very well. Figure 5 presents the frequency response of the backscattering from the same cavity at $\theta = 18°$ (the actual measurement was performed at $\theta = 15°$ and it is reasonable to assume a possible error of 3° might exist). Again the numerical results and measured data [11] agree quite well.

Next we present some results for plane wave scattering by patches (without feeds) residing on or embedded in the substrate in a cavity. Figure 6 shows the aperture field distribution for normal incidence with a patch residing on the surface of the substrate. The bistatic scattering patterns are given in Figure 7 for normal incidence and in Figure 8 for $\theta^i = 45°$, $\phi^i = 0°$. Figures 9-11 show the corresponding results for a patch embedded within the substrate, half way between the top and base of the cavity. The final two sets of plots include aperture field data and scattering patterns for two patches residing

16
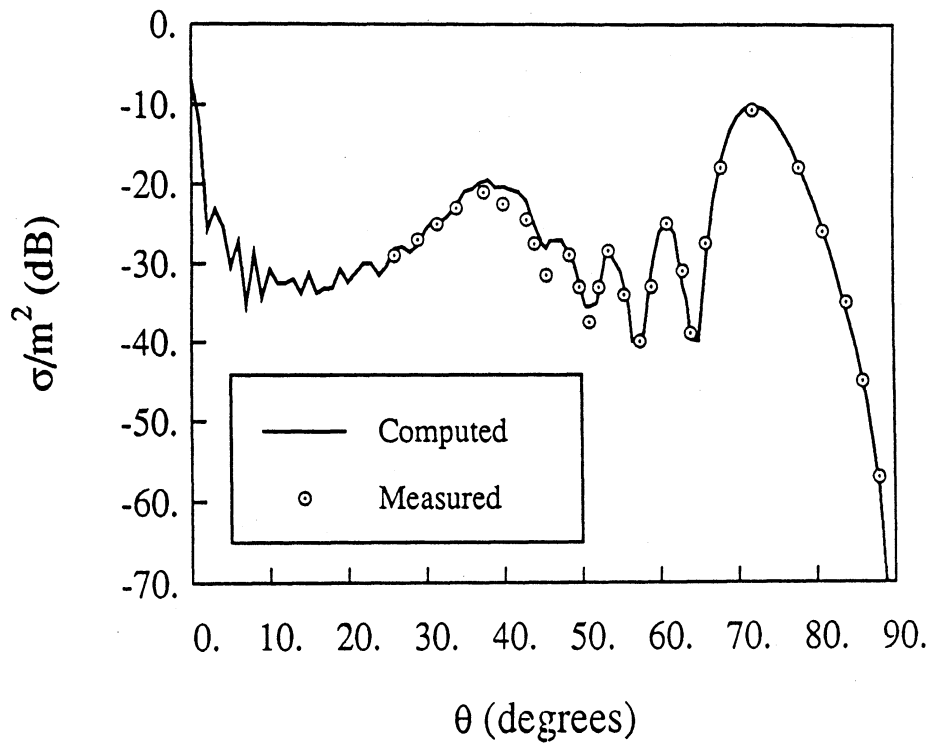
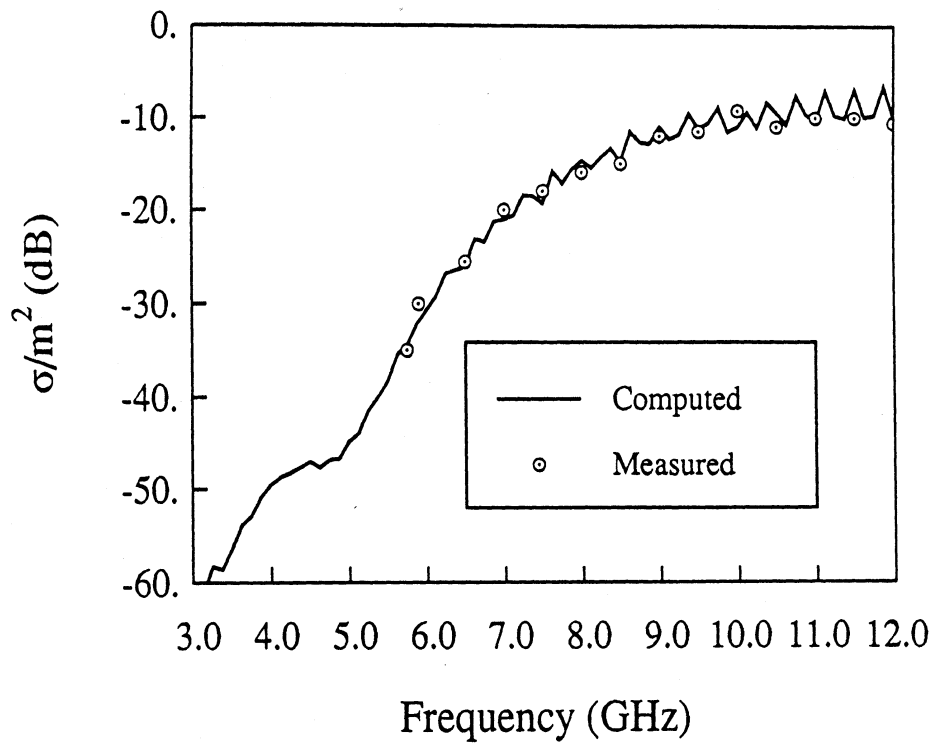Figure 4: Backscatter pattern for a 16 inch long, 0.1968 inch wide and 0.837 inch deep cavity at $f = 12$ GHz.

Figure 5: Backscatter pattern for a 16 inch long, 0.1968 inch wide and 0.837 inch deep cavity with $\theta = 18°$ and $\phi = 0°$.

on the surface or embedded in the substrate, half way between the surface and base of the cavity. In particular Figures 12-15 pertain to the antenna having patches on the substrate surface whereas Figures 16-19 refer to that having both patches embedded in the substrate.

CONCLUSIONS

A hybrid technique was presented which combines the finite element and boundary integral methods for a characterization of the scattering and radiation properties of microstrip patch antennas residing in a cavity. It was found that the technique is efficient and accurate for simulating the geometry. Numerical results were presented for scattering computations demonstrating the validity, versatility and capability of the technique.

TRANSITIONS

The next step in this project is the implementation of the conjugate gradient method in conjunction with the FFT for the solution of the final system. This will make the simulation of large size structures possible. The estimated time for this step is four months. Following this step is the development of various feed models to be incorporated in the computer code and this will take about six months. The resulting code should be capable of characterizing accurately and efficiently the scattering and radiation of finite microstrip structures.

Ex−Ey VECTOR PLOT

Real Part
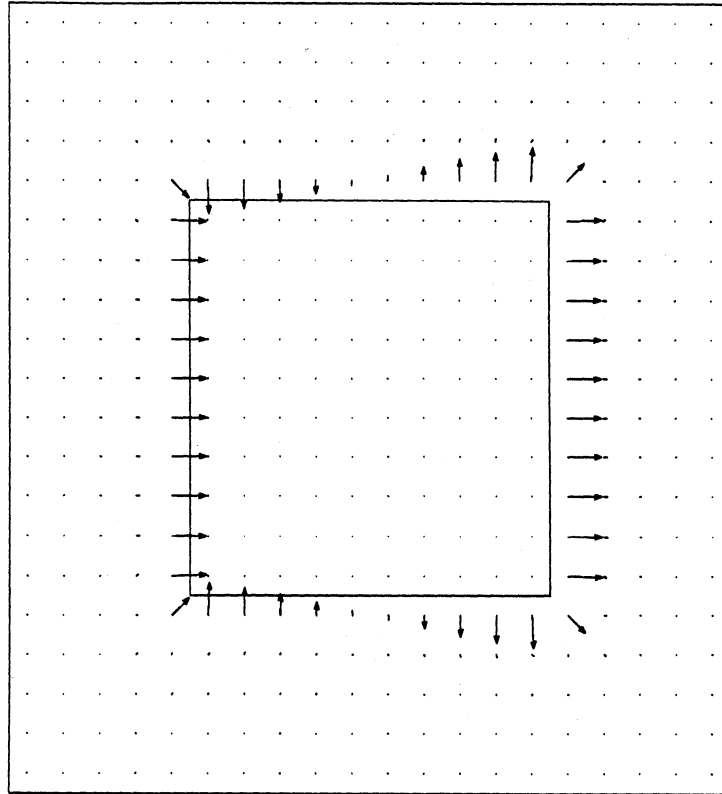
Figure 6: Aperture field (real part) for a patch residing on the surface of the substrate excited with an x-directed normally incident plane wave ($\mathbf{E}^i = \hat{x}E_0$). Cavity size: 3.7 cm $\times$ 3.8 $\times$ 0.16 cm; patch size: 1.85 cm $\times$ 1.9 cm; $\epsilon = 2.22$, $\mu_r = 1$.
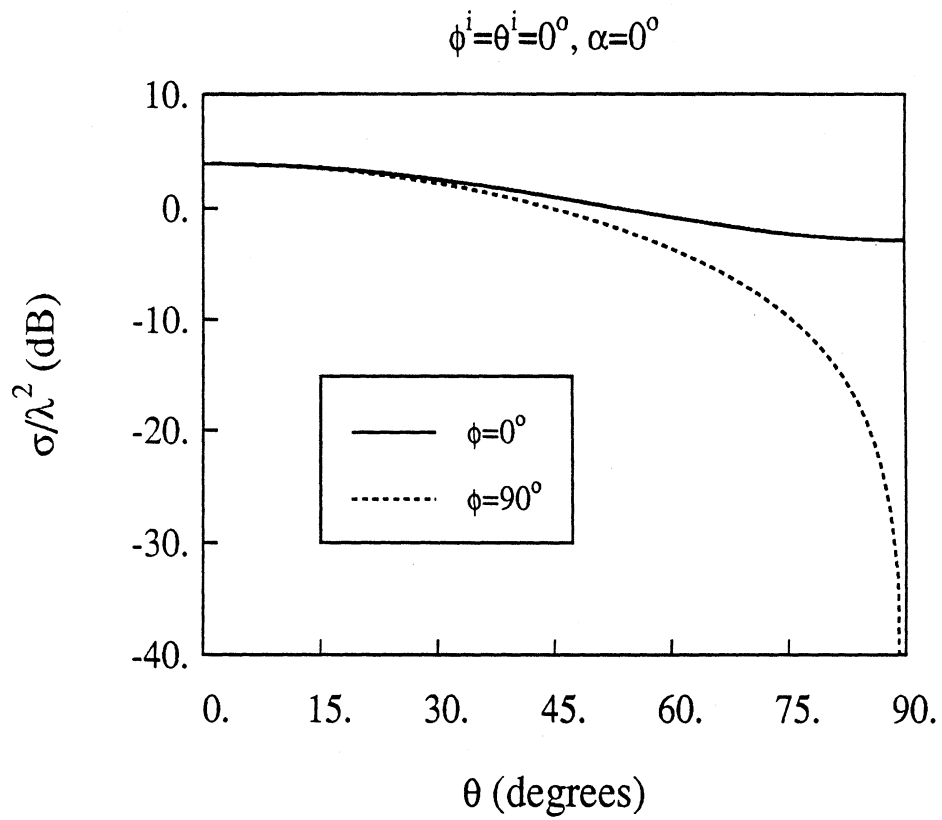
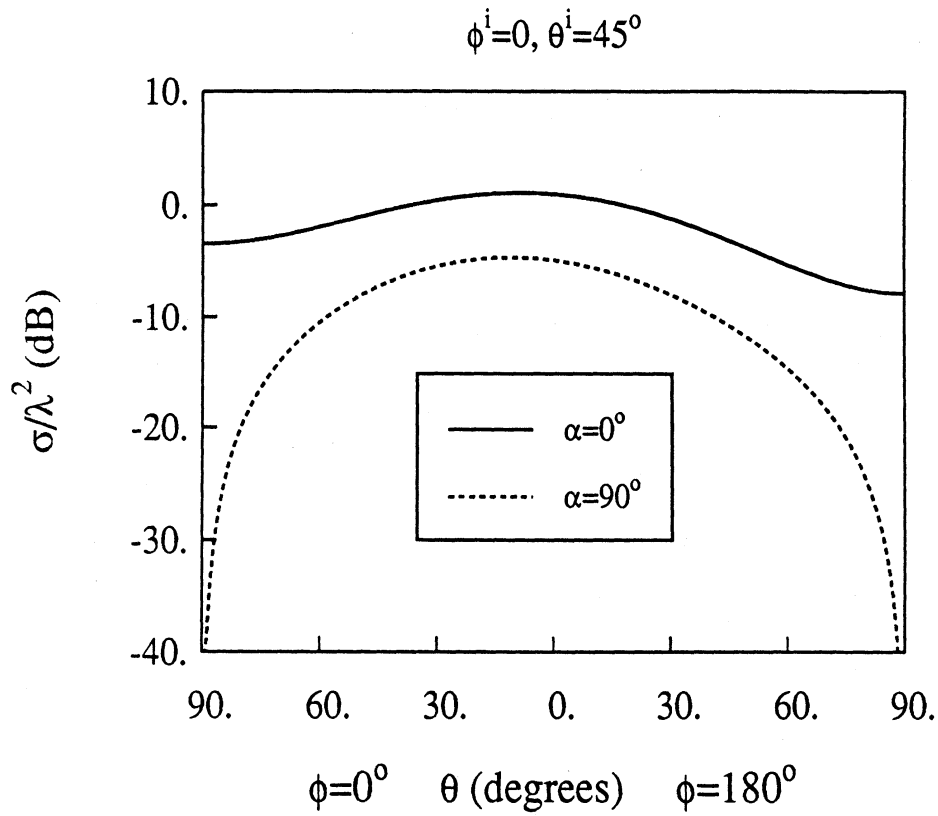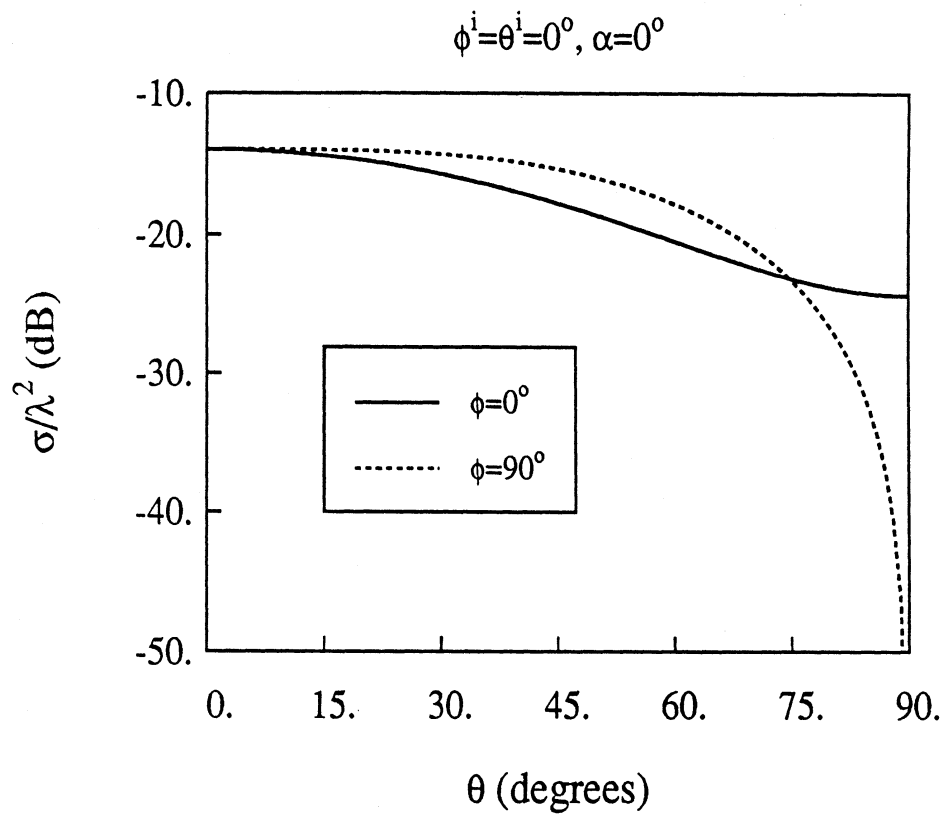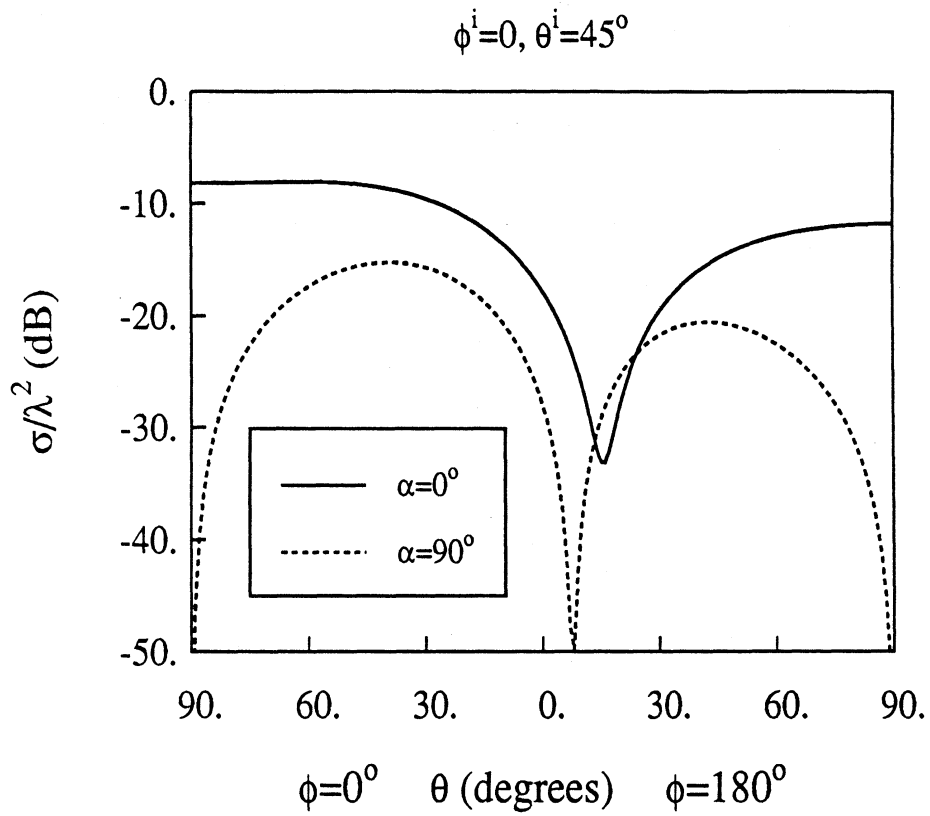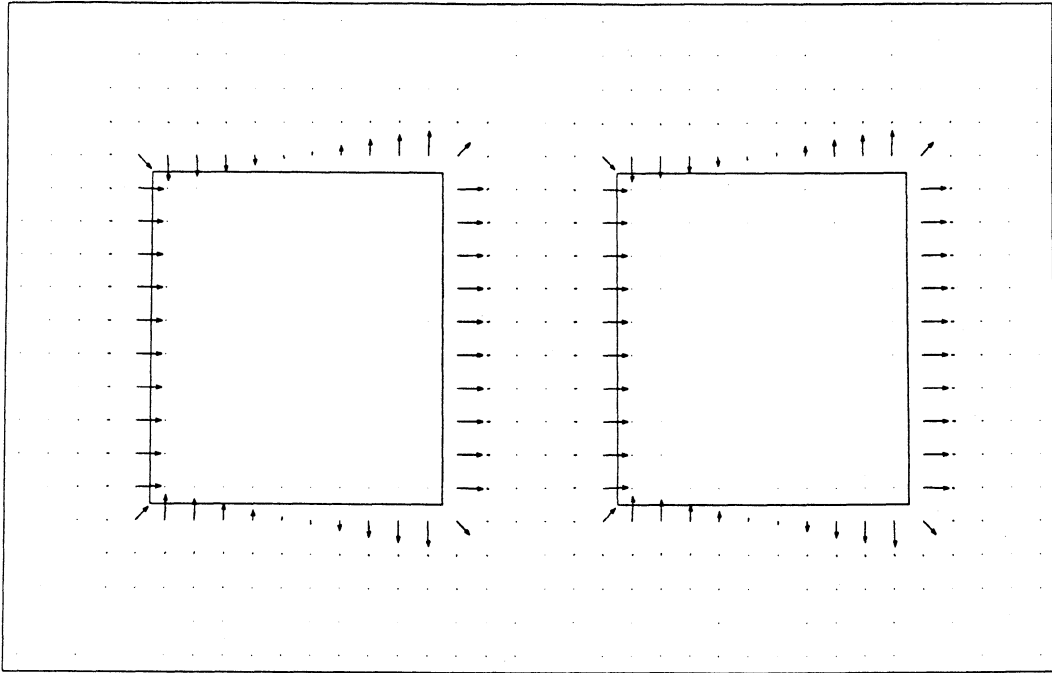Figure 7: Bistatic scattering pattern for the same geometry and excitation as that in Figure 6.

Figure 8: Bistatic scattering pattern for the same geometry as that in Figure 6 corresponding to a plane wave incidence at $\theta^i = 45°$ and $\phi^i = 0°$. $\alpha = 0°$ corresponds to E_θ polarization whereas $\alpha = 90°$ corresponds to E_ϕ polarization.

Ex−Ey VECTOR PLOT
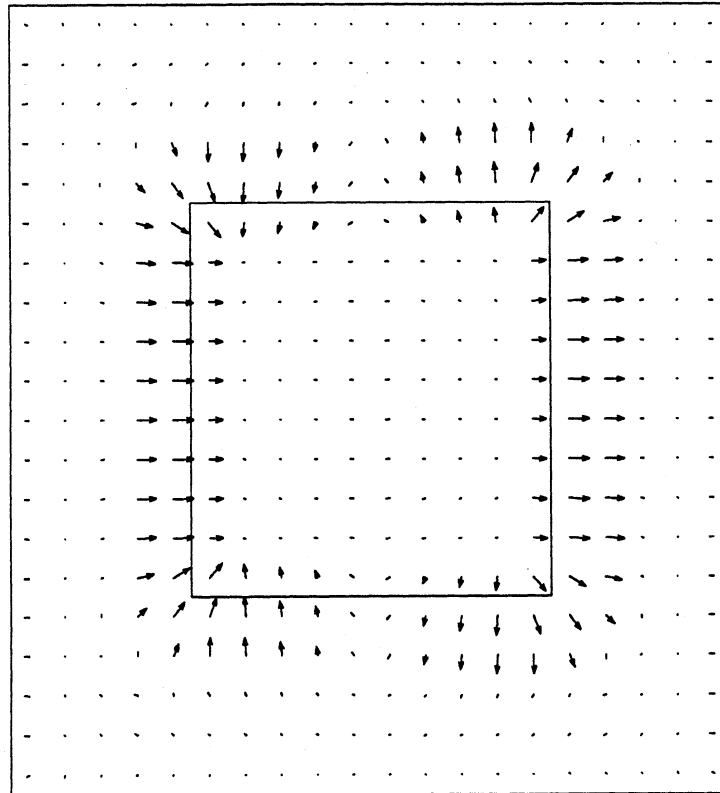
Real Part

Figure 9: Aperture field (real part) for a patch embedded half way between the top and base of the substrate excited with an x-directed normally incident plane wave ($\mathbf{E}^i = \hat{x}E_0$). Cavity size: **3.7 cm × 3.8 × 0.32 cm**; patch size: 1.85 cm × 1.9 cm; $\epsilon = 2.22$, $\mu_r = 1$.

Figure 10: Bistatic scattering pattern for the same geometry and excitation as that in Figure 9.

$\phi^i = 0, \theta^i = 45^o$

Figure 11: Bistatic scattering pattern for the same geometry as that in Figure 9 corresponding to a plane wave incidence at $\theta^i = 45^o$ and $\phi^i = 0^o$. $\alpha = 0^o$ corresponds to E_θ polarization whereas $\alpha = 90^o$ corresponds to E_ϕ polarization.

Ex–Ey VECTOR PLOT
Real Part

Figure 12: Aperture field (real part) for two patches residing on the surface of the substrate excited with an x-directed normally incident plane wave ($\mathbf{E}^i = \hat{x}E_0$). Cavity size: 6.66 cm × 3.8 × 0.16 cm; patch size: 1.85 cm × 1.9 cm; $\epsilon = 2.22$, $\mu_r = 1$.
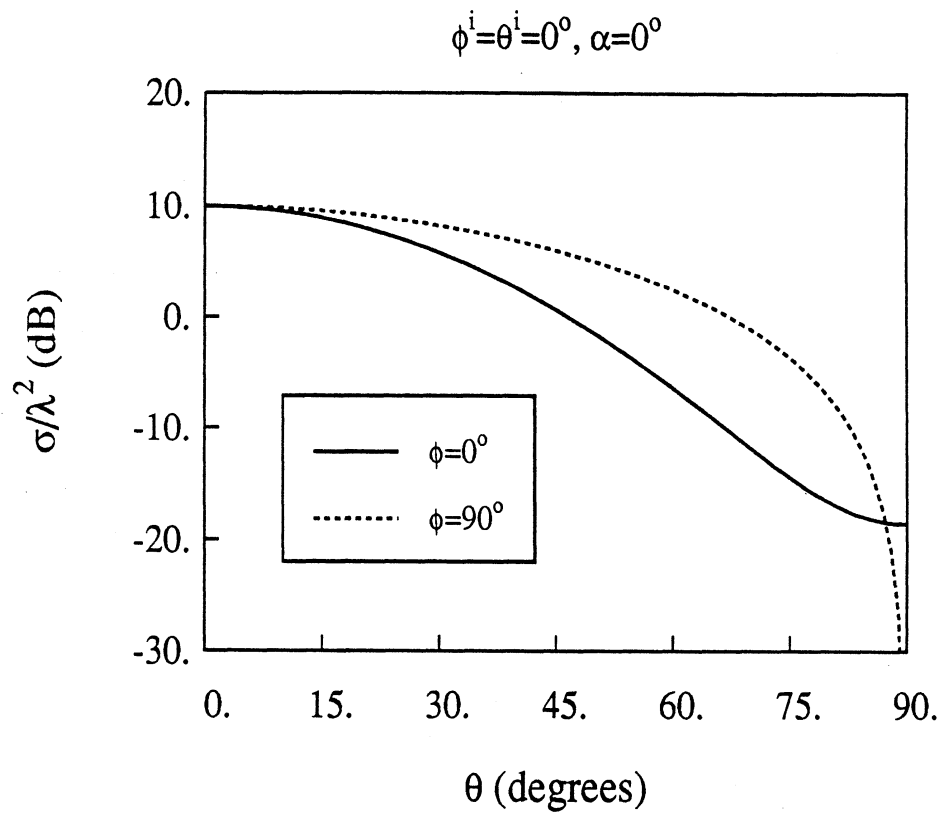
Figure 13: Bistatic scattering pattern for the same geometry and excitation as that in Figure 12.
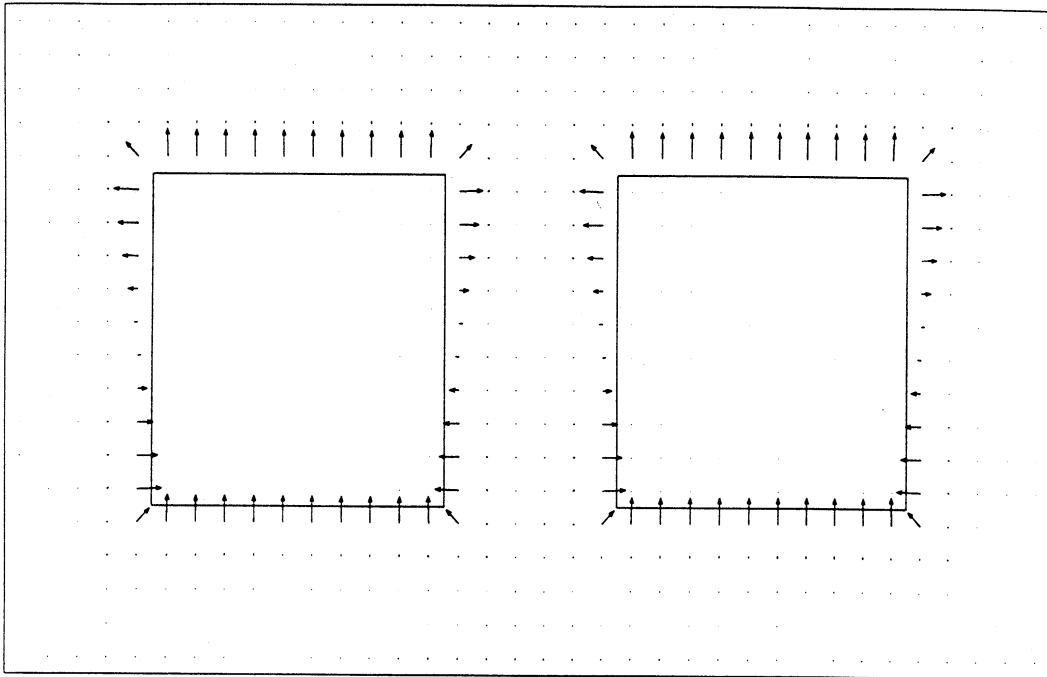
Ex—Ey VECTOR PLOT

Real Part

Figure 14: Aperture field (real part) for two patches residing on the surface of the substrate for excited with a y-directed normally incident plane wave ($\mathbf{E}^i = \hat{y}E_0$). The geometry is the same as that in Figure 12.
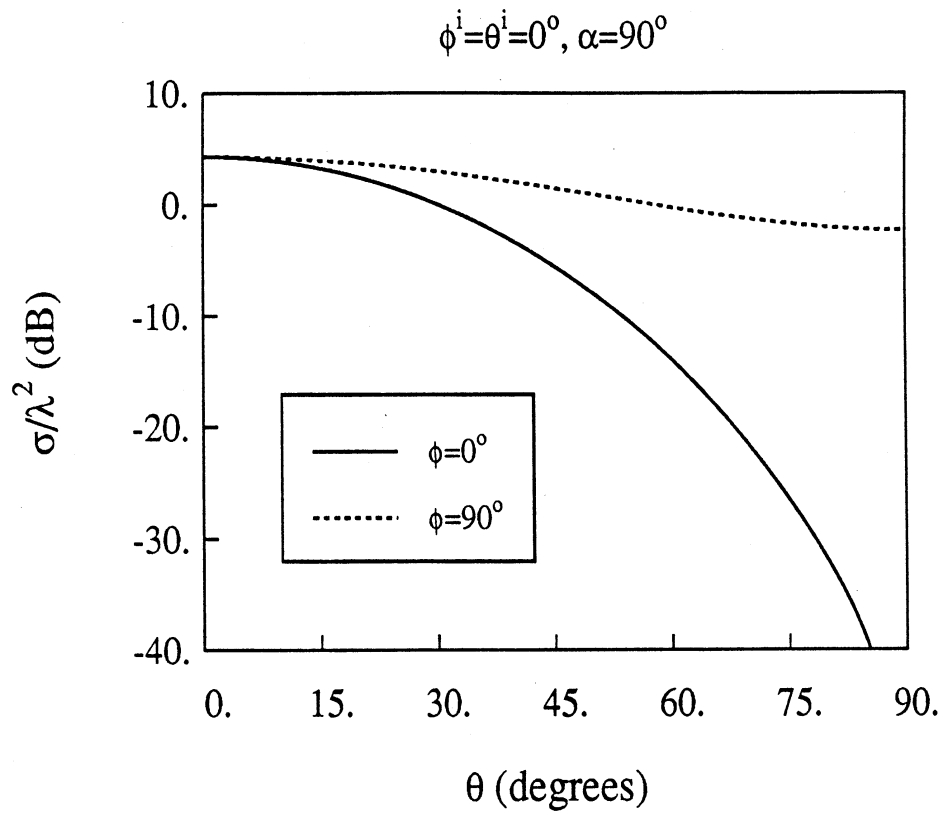
Figure 15: Bistatic scattering pattern for the same geometry and excitation as that in Figure 14.
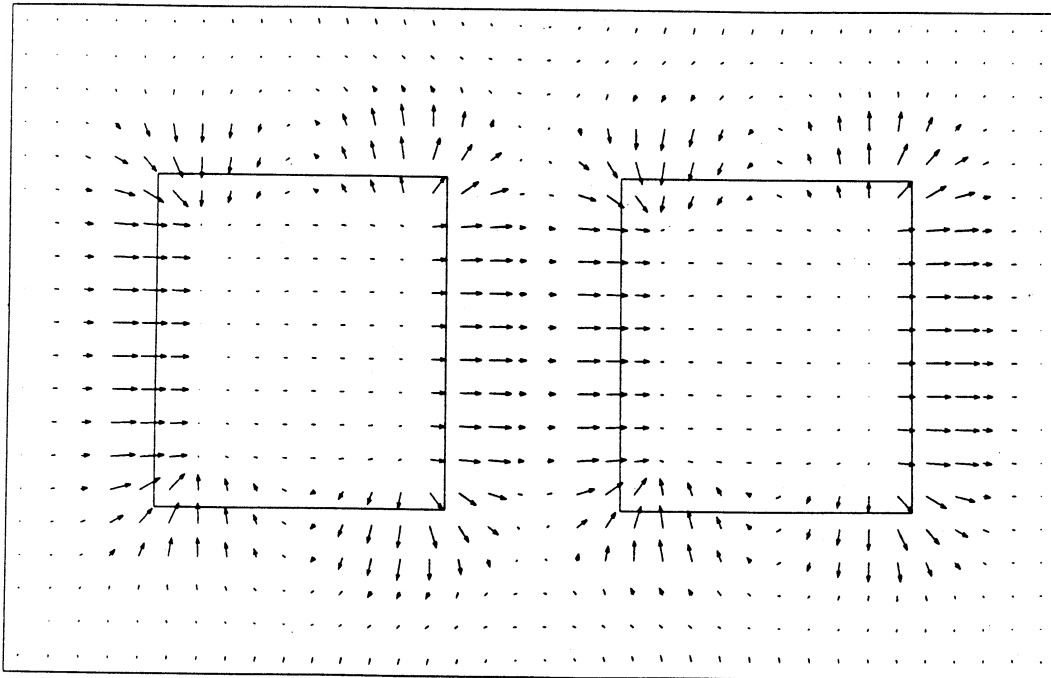
Ex−Ey VECTOR PLOT
Real Part

Figure 16: Aperture field (real part) for two patches embedded half way between the top and base of the substrate excited with an x-polarized normally incident plane wave $(\mathbf{E}^i = \hat{\mathbf{x}}E_0)$. Cavity size: 6.66 cm × 3.8 × 0.32 cm; patch size: 1.85 cm × 1.9 cm; $\epsilon = 2.22$, $\mu_r = 1$.
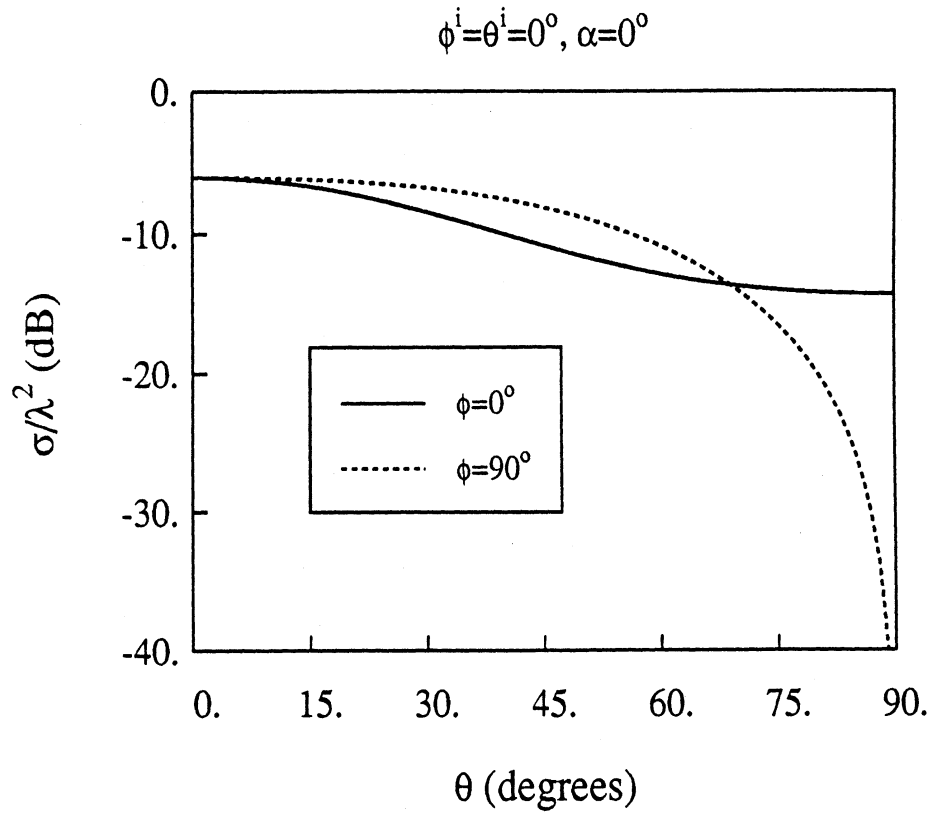
$\phi^i=\theta^i=0°$, $\alpha=0°$

Figure 17: Bistatic scattering pattern for the same geometry and excitation as that in Figure 16.
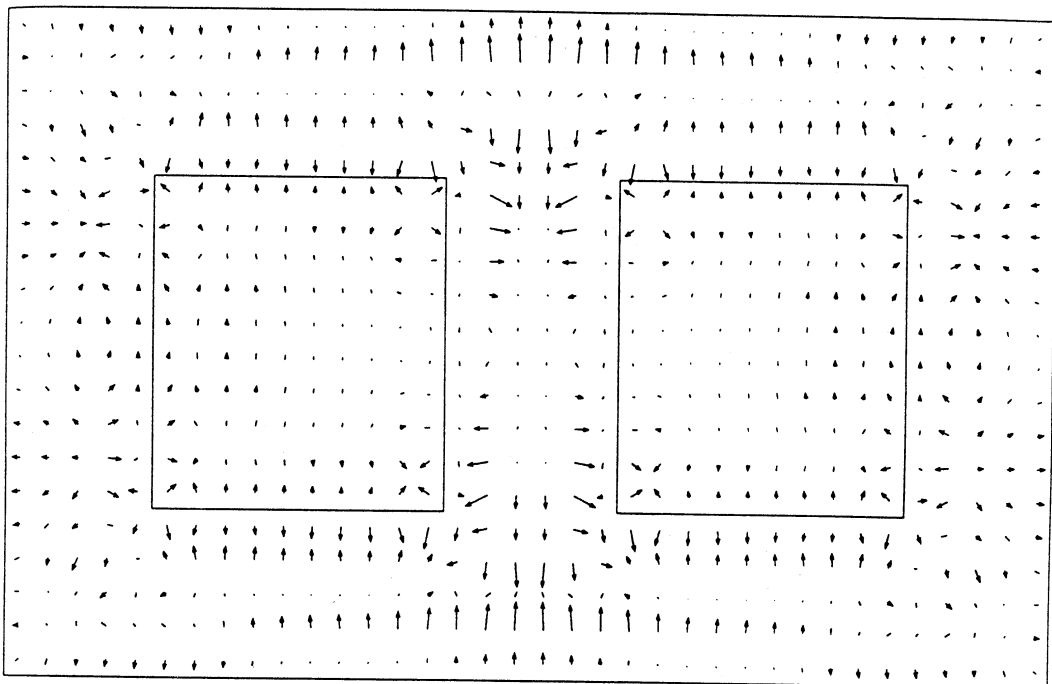
Ex—Ey VECTOR PLOT

Real Part

Figure 18: Aperture field (real part) for two patches embedded half way between the
top and base of the substrate excited with a y-polarized normally incident plane wave
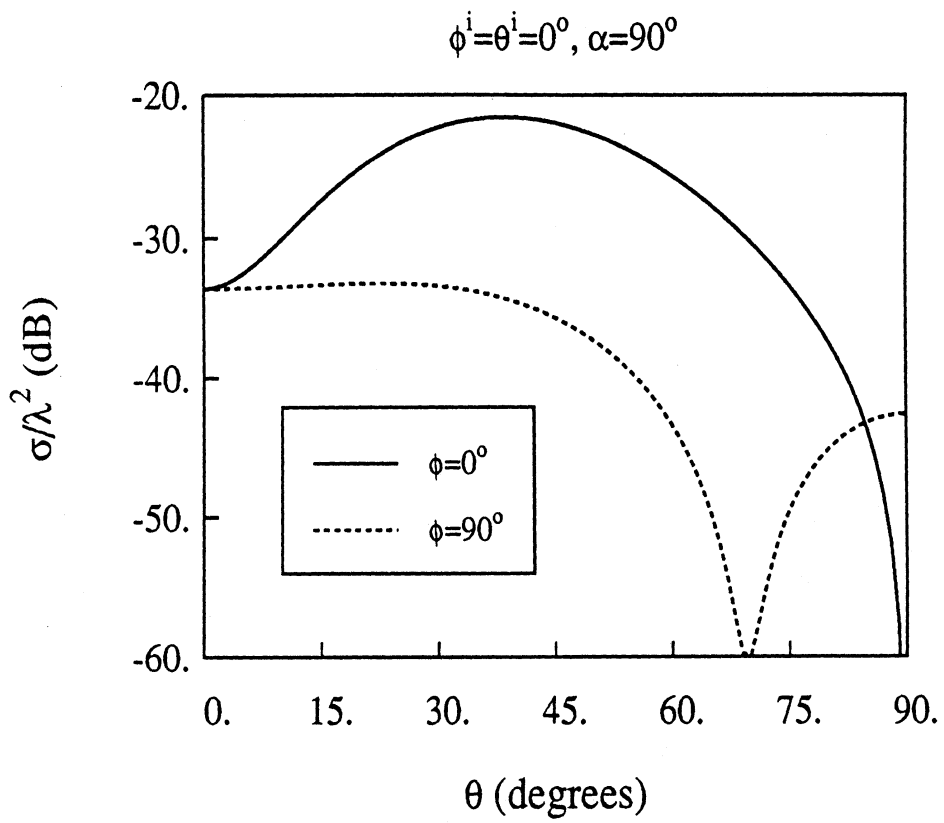($\mathbf{E}^i = \hat{y}E_0$). The geometry is the same as that in Figure 16.

Figure 19: Bistatic scattering pattern for the same geometry and excitation as that in Figure 18.

REFERENCES

[1] J. R. James and P. S. Hall, *Handbook for Microstrip Antennas*. Peter Peregrinus Ltd., 1989.

[2] J. M. Jin and J. L. Volakis, "TE scattering by an inhomogeneously filled aperture in a thick conducting plane," *IEEE Trans. Antennas Propagat.*, vol. 38, pp. 1280-1286, Aug. 1990.

[3] J. M. Jin and J. L. Volakis, "TM scattering by an inhomogeneously filled aperture in a thick conducting plane," *Proc. Inst. Elec. Eng.*, part H, vol. 137, pp. 153-159, Aug. 1990.

4] J. M. Jin and J. L. Volakis, "A finite element – boundary integral formulation for scattering by three-dimensional cavity-backed apertures," *IEEE Trans. Antennas Propagat.*, accepted for publication.

[5] J. M. Jin and J. L. Volakis, "Electromagnetic scattering by and transmission through a three-dimensional slot in a thick conducting plane," *IEEE Trans. Antennas Propagat.*, submitted for publication.

[6] R. F. Harrington, *Time-Harmonic Electromagnetic Fields*. New York: McGraw-Hill, 1961.

[7] O. C. Zienkiewicz, *The Finite Element Method*, 3rd ed. New York: McGraw-Hill, 1977.

[8] J. Van Bladel, "Field singularities at metal-dielectric wedges," *IEEE Trans. Antennas Propagat.*, vol. AP-33, no. 4, pp. 450-455, April 1985.

[9] A. George and J. Liu, *Computer Solutions of Large Sparse Positive Definite Systems.* Englewood Cliffs, NJ: Prentice-Hall, Inc., 1981.

[10] J. M. Jin and V. V. Liepa, "A note on hybrid finite element method for solving scattering problems," *IEEE Trans. Antennas Propagat.*, vol. AP-36, no. 10, pp. 1486-1490, Oct. 1988.

[11] A. K. Dominek, H. T. Shamansky, and N. Wang, "Scattering from three-dimensional cracks," *IEEE Trans. Antennas Propagat.*, vol. AP-37, no. 5, pp. 586-591, May 1989.